J Therm Anal Calorim (2012) 107:877–886
DOI 10.1007/s10973-011-1609-3

Thermal behaviour and electro-optical properties of a series of liquid crystals based on palladium complexes with mixed ligands

Schiff bases and *N*-benzoyl thioureas

Viorel Cîrcu · Ana S. Mocanu · Constantin Roşu · Doina Manaila-Maximean · Florea Dumitraşcu

Received: 27 February 2011 / Accepted: 19 April 2011 / Published online: 7 May 2011

Abstract A series of *ortho*-metallated palladium(II) complexes with two dimeric liquid crystals Schiff base (methoxy and decyloxy as terminal groups) as cyclometallated ligands and *N*-aryl-*N*′-benzoyl thiourea derivatives as co-ligands were prepared and investigated for their liquid crystalline properties. Their structures were assigned based on elemental analysis, FT-IR and ^{1}H NMR spectroscopy while the thermal behaviour was investigated by differential scanning calorimetry and polarising optical microscopy. The complexes with Schiff base ligand bearing methoxy group as terminal group show extensive decomposition during melting while the complexes with Schiff base having decyloxy group as terminal group show monotropic nematic phases, with the mesophase stability strongly related to the type of *N*-aryl-*N*′-benzoyl thiourea derivative used. Their liquid crystalline properties are compared with their analogues having *N*,*N*-dialkyl-*N*′-benzoyl thiourea as co-ligands which were reported previously. One of the latter complexes was also investigated by thermally stimulated depolarisation currents method while the optical transmission was recorded simultaneously. The thermally stimulated depolarisation currents and optical transmission spectra confirmed the previous observation regarding the phase transition temperatures. The current intensity–applied voltage dependencies of this complex were investigated by specific electrical measurements.

Keywords Liquid crystals · Palladium · Orthometallation · *N*-benzoyl thiourea · Imine · Thermally stimulated depolarisation current · *I*–*V* characteristics

V. Cîrcu (✉) · A. S. Mocanu
Department of Inorganic Chemistry, University of Bucharest, 23 Dumbrava Rosie st, sector 2, Bucharest 020464, Romania
e-mail: viorel_carcu@yahoo.com

C. Roşu · D. Manaila-Maximean (✉)
Physics Department II, University "Politehnica Bucuresti", Splaiul Independentei 313, Bucharest 060042, Romania
e-mail: manaila@physics.pub.ro

F. Dumitraşcu
Centre of Organic Chemistry "C. D. Nenitzescu", Romanian Academy, Spl. Independentei 202B, Bucharest 060023, Romania

Introduction

In recent years, there have been a lot of studies dealing with the design of multifunctional liquid crystals because of their great potential in a wide range of applications like sensors, LCDs and OLEDs. Liquid crystalline state has one or more mesophases were they present orientation order and lack (or have only a certain degree of) positional order [1, 2].

Liquid crystalline materials based on metal complexes (metallomesogens) represent one of the best examples where the unique properties of anisotropic fluids are combined with the specific properties of metals, such as colour, polarizability, electrical and magnetic properties. Organometallic compounds of palladium based on *ortho*-metallated complexes with nitrogen-containing heteroaromatic ligands and, in particular, Schiff bases, consisting of both dinuclear and mononuclear organometallic systems, were extensively studied as they offer a unique possibility to tune their physical properties by judicious chemical design [3, 4]. The Schiff bases are commonly used as ligands in the preparation of various metal complexes [5–8]. The α-(4-cyanobiphenyl-4′-oxy)-ω-(4-n-alkyloxyanilinebenzylidene-4′-oxy) hexane Schiff bases compounds used in this work are included in the non-symmetric liquid crystalline dimers category and were reported previously to show SmA and N enantiotropic

phases, with an intercalated arrangement within the SmA phase [9, 10], in which specific molecular interactions between the two different mesogenic units are responsible for this specific phase behaviour. The liquid crystal dimers (also known as dimesogens), composed of either two identical (symmetric) or non-identical (non-symmetric) mesogenic units connected via a flexible central spacer, were largely investigated for their interesting physical properties as well as the possibility to act as model compounds for semi-flexible main-chain liquid crystalline polymers [11].

In this work, the nematogen dinuclear complexes obtained through *ortho*-metallation reaction between such Schiff bases and palladium(II) acetate were used to prepare mononuclear complexes by reacting them with sodium salts of simple *N*-aryl-*N*′-benzoyl thiourea derivatives. Our previous results have shown that mixed-ligands palladium(II) complexes with these type of Schiff bases and *N*,*N*-dialkyl-*N*′-benzoyl thiourea derivatives show liquid crystals properties, with nematic and SmA phases being displayed, the mesomorphic behaviour of such complexes being strongly dependent on the type of the imine ligand employed as well as the type of co-ligand [12]. Indeed, the *N*-benzoyl thiourea derivatives proved to be very good chelating ligands due to the presence of two very strong donor groups (carbonyl and thioamide), reacting with transition metals mostly in monoanionic and bidentate form by deprotonation resulting neutral complexes with S,O-coordination [13–15]. Only few other studies concerning liquid crystals incorporating *N*-benzoyl thiourea moiety were reported previously [16–21], either dealing with purely organic liquid crystals or metallomesogens based on palladium(II) or platinum(II) complexes. The mesomorphic behaviour of mononuclear compounds were investigated by mean of differential scanning calorimetry (DSC) and polarised light microscopy and they will be discussed in connection with the type of *N*-aryl-*N*′-benzoyl thiourea (BTU) derivative used as co-ligand and compare to their analogues bearing *N*,*N*-dialkyl-*N*′-benzoyl thiourea derivatives reported earlier [12]. The DSC technique is one of the most powerful methods for establishing the phase transition in the case of thermotropic liquid crystals [22] and is always used in conjunction with polarised optical microscopy observations. In this study, the DSC measurements of one of the latter complexes are completed with new results obtained by thermally stimulated depolarisation currents (TSDC), a method that can give further insights for the determination of phase transitions often with a better resolution compared to other techniques [23–28]. The shape of the TSDC spectra clearly indicates several peaks corresponding to different processes occurring in the sample during the heating step (depolarisation of permanent dipoles, release of charges, and polarisation changes connected to phase transitions). Also, TSDC method can provide important information regarding the conduction mechanism in the liquid crystalline phase [29, 30].

Results and discussion

The preparation of the two Schiff bases used in this study followed the procedure described already in the literature [9] and is shortly depicted in Scheme 1. They were used further in the *ortho*-metallation reaction with palladium acetate in glacial acetic acid to prepare the dinuclear palladium(II) complexes in moderate to good yields as reported elsewhere [12]. These dinuclear complexes (not shown in Scheme 1) were used in the next step for the preparation of the mononuclear palladium(II) complexes by reacting them with a series of sodium salts of *N*-aryl-*N*′-benzoyl thiourea derivatives (Scheme 1). All the mononuclear palladium(II) complexes are microcrystalline yellow solids, which are stable in normal conditions. Their structure was confirmed by elemental analysis, IR, and ^{1}H NMR spectroscopy. The formation of the *ortho*-metallated mononuclear complexes can be confirmed readily by ^{1}H NMR spectroscopy when a pattern specific to a 1,3,4-substitution of an aromatic ring corresponding to the aldehyde ring of the Schiff base can be seen as two doublets and a doublet of doublets. The presence of the cyanobiphenyl promesogenic unit in the molecule is clearly seen in the IR spectra of all palladium(II) complexes where an absorption band around 2,230 cm^{-1} appears and is assigned to $\nu_{C\equiv N}$. Furthermore, the coordination of BTU derivatives in deprotonated form was confirmed by disappearance of the ν_{NH} frequency in the IR spectra of palladium(II) complexes that suggest the absence of the NH hydrogen, located between the carbonyl and the thiocarbonyl groups of the benzoyl thioureic moiety, information that is further supported by ^{1}H NMR spectroscopy.

These complexes can exist as a mixture of two isomers, depending whether the sulphur atom of the BTU ligand is in *trans* or *cis* position with respect to the nitrogen atom of the imine group of the Schiff base ligand. The ^{1}H NMR spectra indicate for all prepared complexes the presence of only one isomer in solution (one set of signals).

Thermal behaviour

The mononuclear palladium(II) complexes were investigated for their potential liquid crystal properties by hot stage polarised optical microscopy and differential scanning calorimetry. The thermal data are summarised in Table 1. Mesophases were assigned based on their optical texture and one example is presented in Fig. 2. It is very clear that the chain length of the terminal alkoxy group of

Scheme 1 Preparation of mononuclear Pd(II) complexes

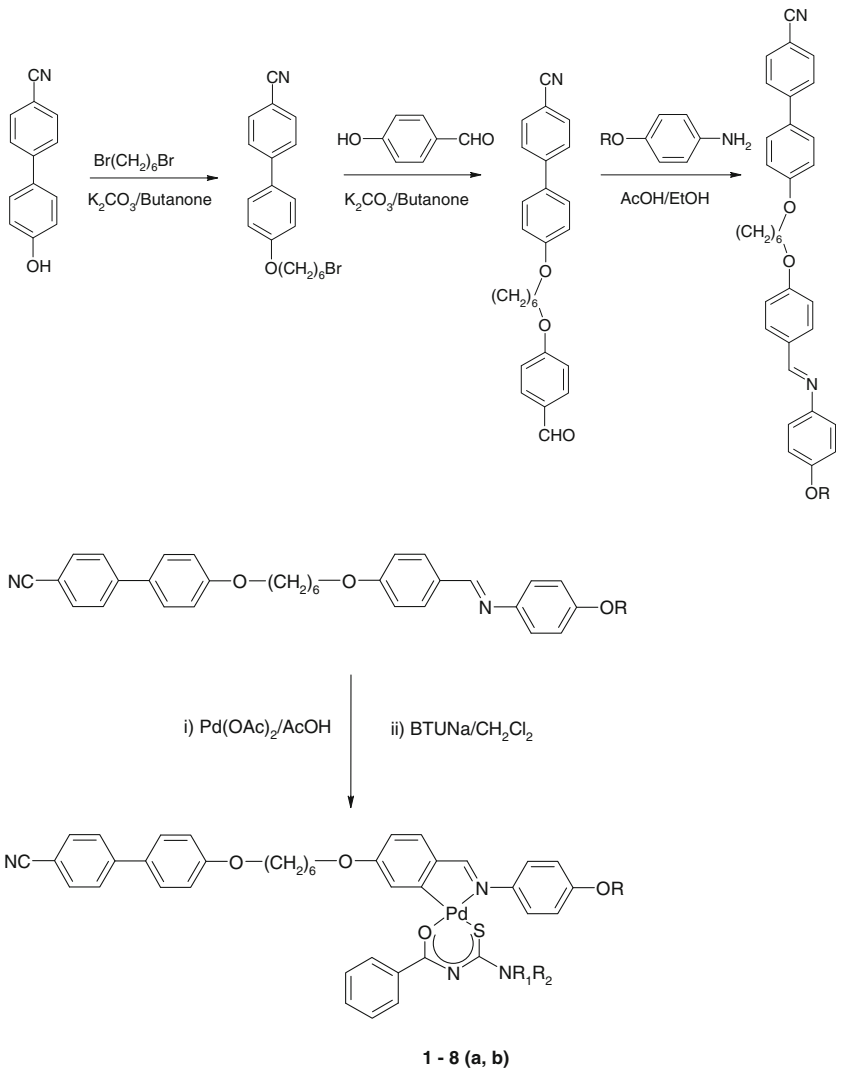

the Schiff bases has a crucial influence on the thermal behaviour of these complexes. Thus, all complexes having Schiff base with methoxy group in terminal position, **1a**–**7a**, show an extensive decomposition concomitant with the melting process that can be easily seen in the DSC traces where a strong exothermic peak follows the endothermic peak corresponding to the melting process (Fig. 1) and confirmed by optical microscopy. The only exception is represented by complex **3a** which, if not heated above 180 °C, shows a monotropic nematic phase on cooling at 117 °C. In this case, it is obvious that the methyl group linked in *meta* position of the aromatic ring from the BTU co-ligand lead to a significant decrease of the melting point, aprox. 22 °C compared to the analogue with methyl group in *para* position, complex **2a,** and 19 °C compared to the analogue bearing unsubstituted aromatic ring, complex **1a**; lowering of the melting point has a clear consequence on avoiding the complex **3a** decomposition at a temperature near to its melting point (Fig. 1).

Table 1 Thermal data for palladium (II) complexes

Compound	Transition	T/°C	ΔH/kJ mol^{-1}	$\Delta S/R$
1a	Cr–I[a]	186	61.0	16.0
1b	Cr–I	160	66.6	18.5
	(I–N)	122[b]		
2a	Cr–I[a]	189	54.0	14.1
2b	Cr–I	164	71.1	19.6
	(I–N)[b,c]	–	–	–
	(N–Cr)	122[b,c]	56.0	17.1
3a	Cr–I	167	40.9	11.2
	(I–N)	117	1.7	0.5
	Tg	58	–	–
3b	Cr–I	156	84.3	23.6
	(I–N)	117	2.2	0.7
	Tg	36	–	–
4a	Cr–I[a]	193	50.6	13.1
4b	Cr–Cr′	139	21.2	6.2
	Cr′–N	–	–	–
	N–I	152[d]	17.7[d]	5.0
	I–N	151	2.7	0.8
5a	Cr–I[a]	197	73.2	18.7
5b	Cr–N	–	–	–
	N–I	140[d]	50.1[d]	14.6
	I–N	139	2.0	0.6
6a	Cr–I[a]	198	58.6	15.0
6b	Cr–Cr′	122	5.5	1.7
	Cr′–I	153	47.2	13.3
	(I–N)	116[b]	–	–
7a	Cr–I[a]	174	38.4	10.3
7b	Cr–I	152	70.0	19.8
	(I–N)	132[b]	–	–
8b[e]	Cr–Cr′	104	12.9	4.1
	Cr′–N	118	33.6	10.3
	N–I	138	1.6	0.5

[a] This transition is followed by decomposition

[b] Values taken from microscopy

[c] Transition occured just before crystallization

[d] Combined enthalpies

[e] Taken from [12]

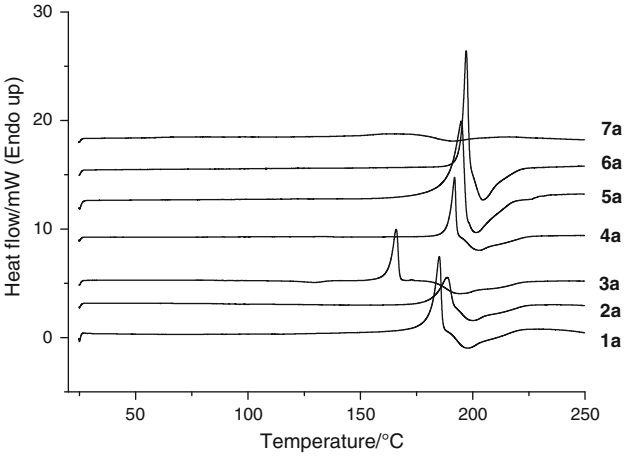

Fig. 1 The DSC traces of complexes **1a–7a** showing their melting followed by decomposition

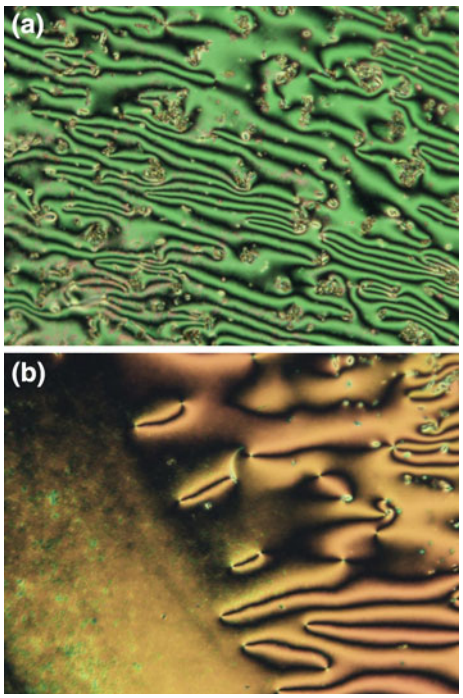

Fig. 2 Two pictures taken at the polarised optical microscope of the nematic phase of complex **5b** at 137 °C (**a**) and at 125 °C (**b**)

On the other hand, regarding the remainder of the materials, the Pd(II) complexes with Schiff base having decyloxy as terminal group (**1b–7b**), all of them exhibit a monotropic nematic phase, which was identified on the basis of the characteristic Schlieren optical texture that show two- and four-brushes singularities observed when viewed under the polarised light microscope; this texture also flashed under mechanical stress (Fig. 2). Here, it is important to mention that for complexes **1b**, **2b**, **6b** and **7b** it was impossible to detect the peak corresponding to the transition from the isotropic to nematic phase on the DSC traces, such transition being associated with a very weak enthalpic effect. This phase transition was evidenced only by microscopy observations.

The complex **1b** could be a useful starting point in discussing the mesogenic properties of complexes **1b–7b**, as it contains the unsubstituted *N*-benzoyl-*N*′-phenyl thiourea ligand. This complex shows a relative high melting point, 160 °C, and a strong enantiotropic nematic phase that is stable over a little range before crystallization

occurs. In our previous studies [19–21], we proposed several reasons for such a behaviour that are related to the high flexibility of the structure adopted by this type of ligands resulting in a less favourable molecular shape from the liquid crystalline molecular design point of view together with the intramolecular hydrogen bonds N–H···S, that could be formed between the S atom of the thiocarbonyl group and the hydrogen atom of the amino –NHR group of the BTU ligand.

The next step was to introduce several new BTU derivatives that contain one phenyl ring substituted with various groups with the aim of establishing some structure–properties correlations. It was found that, with the exception of complex **2b** for which the melting point is 4 °C higher than that of complex **1b,** the melting points of all other complexes were not highly affected by the introduction of different groups in the BTU molecule and are lowered by 3–8 °C compared to complex **1b**. Complex **3b** shows, by cooling during the first heating–cooling cycle, a monotropic nematic phase that follows the isotropic state. The former can be further cooled to a glassy state with $T_g = 36$ °C (Fig. 3a). When this sample is subjected to the second heating process, two successive crystallization peaks can be seen in the range 75–110 °C (Fig. 3b) before the melting one, around 160 °C, confirming the monotropic nature of mesophase. On the other hand, the stability of nematic phase is related to the size and polarity of the group attached to the phenyl ring of BTU derivative. The highest stability is seen for complex **4b** that contains BTU co-ligand with methoxy group in *para* position. Moreover, the nematic phase of complex **4b** is enantiotropic as it is for complex **5b** that contains fluorine group. Such a behaviour is similar to that observed for other type of palladium(II) complexes with the same BTU derivatives but different Schiff base with two alkoxy groups instead of cyanobiphenyl promesogenic unit [21], when such a tendency was a consequence of the polarity of the lateral substituent located on the BTU co-ligand combined with a space-filling effect [31].

An interesting feature is given rise by comparing the thermal behaviour of complexes **1b–7b** with that of the palladium(II) analogues **8b** bearing *N*,*N*-dialkyl-*N*′-benzoyl thiourea derivatives which were reported elsewhere [12]. While most of the complexes in the present study (**1b–7b**) show a narrow range monotropic nematic phase, their Pd(II) analogues having *N*,*N*-dialkyl-*N*′-benzoyl thiourea derivatives show only an enantiotropic nematic phase with a much higher thermal stability and with melting and clearing points that are influenced by the chain length of the corresponding BTU derivative (see Fig. 4). The explanation for such a behaviour could be also related to the much less favourable molecular shape adopted by

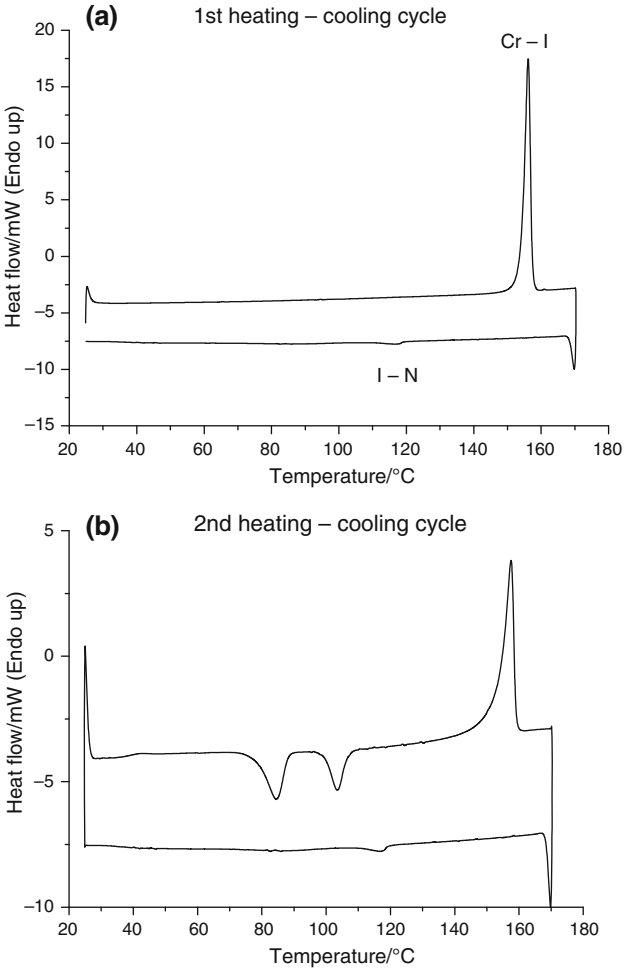

Fig. 3 The DSC traces showing the first (**a**) and the second (**b**) heating–cooling cycles for compound **3b**

complexes with *N*-aryl-*N*′-benzoyl thiourea derivatives, as mentioned above.

TSDC and electro-optical measurements

We chose to record the TSDC and electro-optical measurements for complex **8b** which has a broader mesomorphic range (approx. 20 °C) and lower transition temperatures, as well as a very high thermal stability (see Fig. 4).

The schematic representation of the heating–cooling cycles applied to the sample during the TSDC measurements can be seen in Fig. 5 [32, 33]. In the preliminary heating step (0), from room temperature to a pre-established temperature (T_p), higher than the nematic–isotropic transition temperature of the liquid crystal, initial depolarisation of the sample takes place. In the steps 1, 2 and 3 there is no polarising field ($E_p = 0$); these steps are

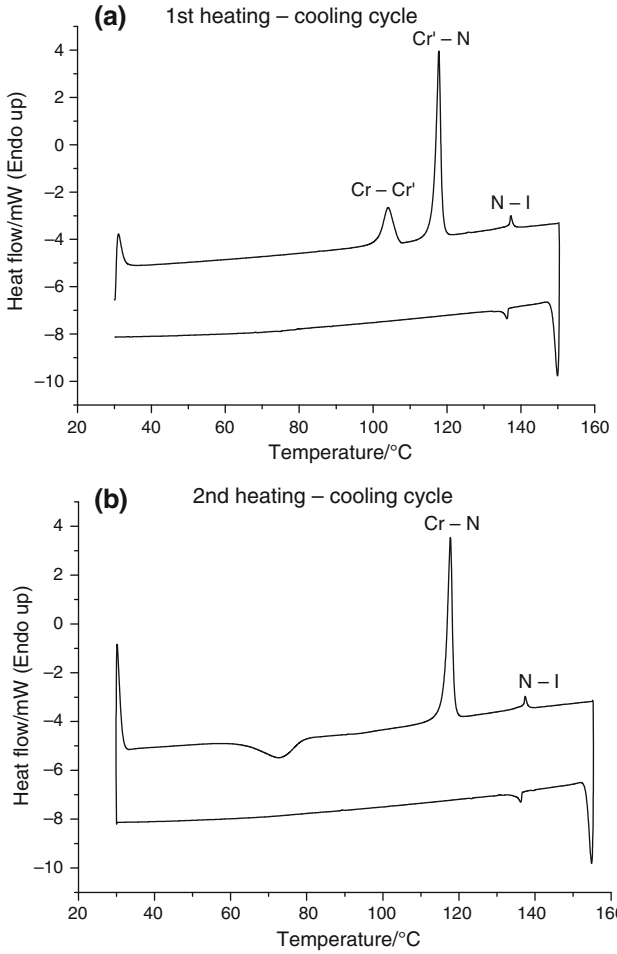

Fig. 4 The DSC curve corresponding to complex **8b** (first (**a**) and second (**b**) heating–cooling cycles)

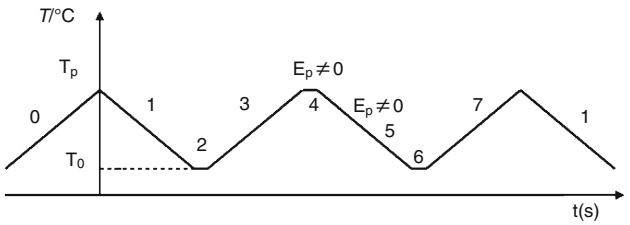

Fig. 5 Schematic representation of the heating–cooling cycles applied to complex **8b** during TSDC measurements

performed to eliminate residual charges, induced by previous treatments applied on the sample.

During step 4, at T_p, the polarising field $E_p = U_p/g$ is applied, (U_p is the voltage applied on the sample and g is the thickness of the sample) and it is maintained during the cooling down to T_0 (step 5). During the step 6, the field E_p is cut-off and the sample is short-circuited to eliminate capacitive discharge. The depolarising currents (TSDC spectra) are registered during step 7. The heating–cooling rates were of 1 °C/min while the duration of steps 2, 4 and

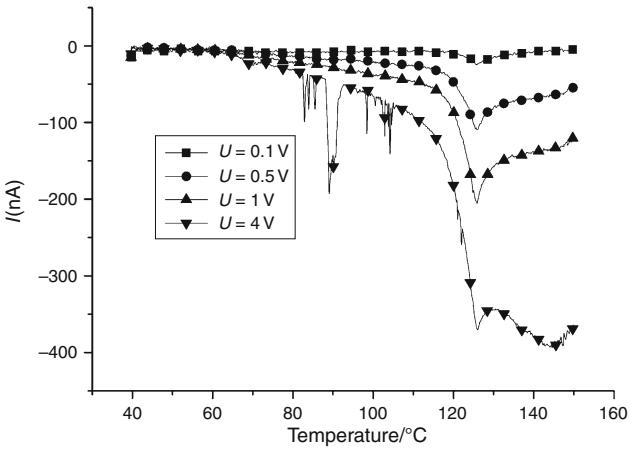

Fig. 6 The TSDC spectra of the complex **8b** registered in step 7, after applying different polarising electric fields on the sample (The density of measurement point represented on the graph is reduced)

6 were of 15 min. For complex **8b**, the polarisation temperature (T_p) was 150 °C while $T_0 = 40$ °C.

The TSDC spectra of the complex **8b**, measured in step 7 after applying different voltages are depicted in Fig. 6.

All TSDC spectra show a peak (in absolute value) at about 122 °C that corresponds to the very distinct Cr–N transition. This transition involves a high energy and the corresponding intensity peak overlaps the N–I peak, with the exception of the curve registered after the highest pre-applied electric field, that shows a distinct second broad peak that is assigned to the N–I transition. The Cr–N transition peak is very sharp and it has been more rarely registered in this type of TSDC measurements. For example, in a previous TSDC study on a liquid crystalline organometallic palladium complex based on 4,4′-dihexyloxyazoxybenzene and acetylacetonate as co-ligand, this transition was not detected, being totally overlapped by the N–I corresponding peak [29].

Using the Arrhenius curve presented in Fig. 7, the value of the activation energy was found to be $E = 0.831$ eV, practically the same regardless the temperature.

The optical transmission measured in step 7, simultaneously with the thermally stimulated currents, is presented in Fig. 8. The optical transmission is expressed in percent (considering 100% for a perfect transparent sample and 0% for a completely opaque one). A relatively high optical transmittance was observed in the 40–60 °C temperature range, when the complex **8b** is in a supercooled nematic mesophase. The optical transmission in this temperature range is greater after higher pre-applied electric fields, implying a higher degree of order. At about 60 °C, there is an abrupt decrease in the optical transmission corresponding to the transition to a non-birefringent crystalline state. Further heating of the sample results in a strong increase of the optical signal at around 125 °C,

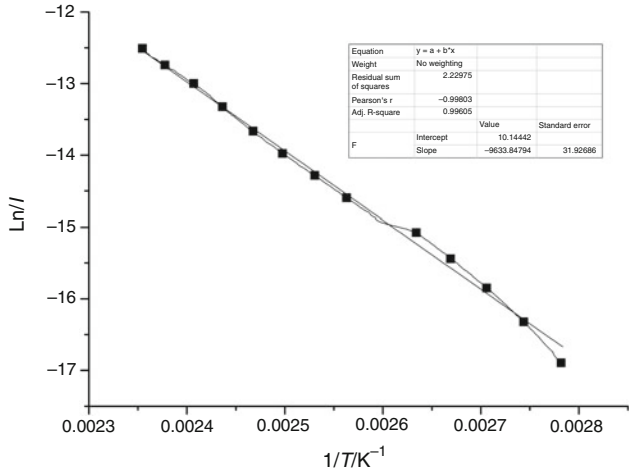

Fig. 7 The Arrhenius curve determined in step 7, on cooling, for complex **8b**, for an applied voltage of 1 V

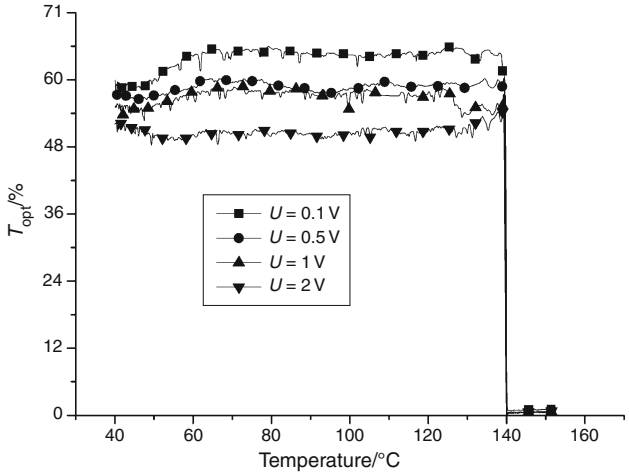

Fig. 9 Optical transmission of complex **8b** measured in step 5 (cooling with applied electric field).

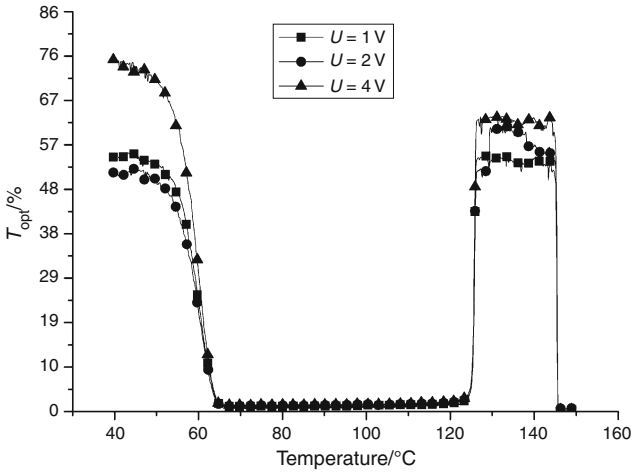

Fig. 8 Optical transmission of complex **8b** measured in step 7 (heating without electric field). The pre-applied voltages, in step 4 and 5, are marked on the graph

concomitant with the transition from the crystalline state to the nematic phase. The transition N–I can be easily seen at about 140 °C when the transmission drops nearly zero confirming the thermal behaviour seen on the second cycle of heating in the DSC curve (Fig. 4b).

Figure 9 shows the optical transmission of **8b** measured in step 5. The compound passes from isotropic to nematic around 140 °C, and it remains in the nematic state until the room temperature. Again, there is a slight increase of the optical transmission with the applied electric field, due to a better orientation of the molecules. The current intensity (*I*)—applied voltage (*U*) plots, *I*(*U*), for different voltages ranging between −40 and +40 V were recorded both on heating and cooling steps. The results are presented in Fig. 10a for heating step and in Fig. 10b for the cooling step

As it can be seen, the dependence is practically ohmic for the curves registered for lower applied electric fields (−20 V, +20 V); at higher electric fields, especially for relative higher temperatures, a nonlinear dependence is much more pronounced. Obviously, as temperature increases, the electrical conductivity of the sample also increases; this can be correlated with the decrease of the viscosity, leading to a higher mobility of electrically charged carriers.

The slopes of the curves registered at 60 °C are pretty different when measured during the heating or cooling steps. This difference is related to thermodynamic stability of the nematic phase. Thus, on cooling the sample from the isotropic liquid to 60 °C, a supercooled nematic phase is present in this temperature range, which is correlated with a lower electrical resistance than the one corresponding to the crystalline state which is present when the sample is heated from the room temperature.

Experimental

Dichloromethane was distilled from phosphorus pentaoxide; the other chemicals were used as supplied.

^{1}H NMR spectra were recorded on a Varian Gemini 300 BB spectrometer operating at 300 MHz, using $CDCl_3$ as solvent. ^{1}H chemical shifts were referenced to the solvent peak position, δ 7.26 ppm.

The phase assignments and corresponding transition temperatures for the palladium(II) complexes were determined by optical-polarised light microscopy using a Nikon 50iPol microscope equipped with a Linkam THMS600 hot stage and TMS94 control processor. Temperatures and enthalpies of transition were obtained by DSC employing a Diamond DSC Perkin Elmer. The materials (between 2 and

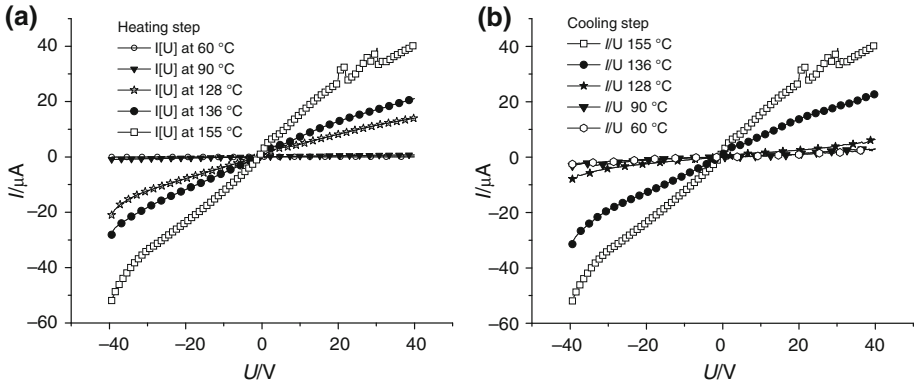

Fig. 10 The current intensity (I) as a function of applied voltage (U) for complex **8b**: (**a**) during the heating step at the temperatures: 60, 90, and 110 °C (crystalline phase), 128 °C (nematic phase), 136 °C (nematic phase) and 155 °C (isotropic state); (**b**) on cooling at 155 °C (isotropic phase) and 136 °C–60 °C corresponding to the nematic phase in its supercooled state

4 mg) were studied at scanning rates of 5 and 10 °C/min after being encapsulated in aluminium pans. Two or more heating/cooling cycles were performed on each sample that showed liquid crystalline properties. Mesophases were assigned by their optical texture [34].

The experimental set-up for TSDC measurements has been described in detail elsewhere [35]. In order to perform the TSDC and electro-optical measurements, the complex **8b** was filled in a 12 μm thick ITO covered sandwich glass cell by capillarity. The optical transmission experiment was performed in the following way: the optical beam from a light source was transmitted through the cell and measured by the photomultiplier; crossed polarizers have been used. The $I(U)$ measurements were made by using a Keithley 2400 electrometer and a temperature-controlled hot stage Metler-Toledo 3200 series.

The synthesis of the two Schiff bases and of the dinuclear palladium(II) complexes was carried out as described elsewhere [9, 12]. The *N*-benzoyl thiourea derivatives as well as their sodium salts used in this work were prepared according to the methods published in literature [19, 36].

Synthesis of mononuclear palladium(II) complexes

The solid sodium salt of *N*-aryl-*N*′-benzoyl thiourea derivative (0.30 mmol) was added to a solution of the corresponding binuclear complex (0.10 mmol) in CH_2Cl_2 (15 ml) and the resulting mixture was stirred at room temperature for 1 day. The solvent was removed and the solid was purified on silica using CH_2Cl_2 as eluant. The crude yellow solid was recrystallised from a mixture of CH_2Cl_2/C_2H_5OH (1/1) at −25 °C in the case of palladium(II) complexes.

The yields, elemental analysis results as well as ^{1}H NMR and IR data are presented below:

1a Yield 51%, yellow crystals. Anal. Calcd for $C_{47}H_{42}N_4O_4PdS$: C, 65.2; H, 4.9; N, 6.5; Found: C, 64.8; H, 5.3; N, 6.3.

^{1}H NMR (300 MHz, $CDCl_3$): 8.12 (s, 1H), 7.74–7.51 (m, 12H), 7.42–7.34 (m, 5H), 7.22 (m, 2H), 7.03–6.98 (m, 4H), 6.90 (d, 1H, ^4J = 2.4 Hz), 6.60 (dd, ^3J = 8.4 Hz, ^4J = 2.4 Hz, 1H), 4.04 (m, 4H), 3.89 (s, 3H), 1.85 (m, 4H), 1.60 (m, 4H).

IR (cm^{-1}): 2232w($\nu_{C\equiv N}$); 1598, 1578s($\nu_{C=N}$); 1538, 1504, 1418vs(ν_{CN+CS}), 1246vs(ν_{CN}).

1b. Yield 88%, yellow crystals. Anal. Calcd for $C_{56}H_{62}N_4O_4PdS$: C, 67.8; H, 6.1; N, 5.7; Found: C, 67.5; H, 6.4; N, 5.5.

^{1}H NMR (300 MHz, $CDCl_3$): 8.12 (s, 1H), 7.75–7.51 (m, 12H), 7.39 (m, 5H), 7.22 (m, 2H), 6.99 (m, 4H), 6.89 (s br, 1H), 6.60 (dd, ^3J = 8.1 Hz, ^4J = 2.4 Hz, 1H), 4.04 (m, 6H), 1.83 (m, 6H), 1.62–1.30 (m, 18H), 0.89 (t, ^3J = 6.5 Hz, 3H).

IR (cm^{-1}): 2226w($\nu_{C\equiv N}$); 1601, 1580s($\nu_{C=N}$); 1538, 1495, 1416vs(ν_{CN+CS}), 1249vs(ν_{CN}).

2a. Yield 72%, yellow crystals. Anal. Calcd for $C_{48}H_{44}N_4O_4PdS$: C, 65.6; H, 5.0; N, 6.4; Found: C, 65.3; H, 5.4; N, 6.3.

^{1}H NMR (300 MHz, $CDCl_3$): 8.12 (s, 1H), 7.73 (d br, 2H), 7.64 (m, 4H), 7.53 (AA′BB′ system, ^3J = 8.8 Hz, 2H), 7.45–7.33 (m, 6H), 7.25–7.15 (m, 4H), 7.05–6.97 (m, 4H), 6.90 (s br, 1H), 6.60 (dd, ^3J = 7.9 Hz, ^4J = 2.4 Hz, 1H), 4.04 (t, ^3J = 6.3 Hz, 4H), 3.89 (s, 3H), 2.36 (s, 3H), 1.85 (m, 4H), 1.58 (m, 4H).

IR (cm^{-1}): 2224w($\nu_{C\equiv N}$); 1603, 1579s($\nu_{C=N}$); 1539, 1505, 1419vs(ν_{CN+CS}), 1247vs(ν_{CN}).

2b. Yield 65%, yellow crystals. Anal. Calcd for $C_{57}H_{62}N_4O_4PdS$: C, 68.1; H, 6.2; N, 5.6; Found: C, 67.8; H, 6.6; N, 5.3.

^{1}H NMR (300 MHz, $CDCl_3$): 8.13 (s, 1H), 7.73 (d br, 2H), 7.64 (m, 4H), 7.53 (AA′BB′ system, ^3J = 8.8 Hz, 2H), 7.45–7.33 (m, 6H), 7.25–7.15 (m, 4H), 6.99 (t, AA′BB′ system, ^3J = 8.5 Hz, 4H), 6.90 (s br, 1H), 6.60 (dd, ^3J = 7.9 Hz, ^4J = 2.4 Hz, 1H), 4.09–4.01 (m, 6H), 2.36 (s, 3H), 1.85 (m, 6H), 1.62–1.28 (m, 18H), 0.89 (t, ^3J = 6.5 Hz, 3H).

IR (cm^{-1}): 2226w($\nu_{C\equiv N}$); 1601, 1579s($\nu_{C=N}$); 1535, 1505, 1419vs(ν_{CN+CS}), 1237vs(ν_{CN}).

3a. Yield 62%, yellow crystals. Anal. Calcd for $C_{48}H_{44}N_4O_4PdS$: C, 65.6; H, 5.0; N, 6.4; Found: C, 65.2; H, 5.3; N, 6.2.

^{1}H NMR (300 MHz, $CDCl_3$): 8.13 (s, 1H), 7.75 (d br, 2H), 7.64 (m, 4H), 7.53 (AA′BB′ system, $^3J = 8.8$ Hz, 2H), 7.45–7.33 (m, 7H), 7.25–7.21 (m, 3H), 7.00 (m, 4H), 6.91 (s br, 1H), 6.60 (dd, $^3J = 8.3$ Hz, $^4J = 2.4$ Hz, 1H), 4.07–4.01 (m, 4H), 3.90 (s, 3H), 2.38 (s, 3H), 1.85 (m, 4H), 1.59 (m, 4H).

IR (cm^{-1}): 2224w($\nu_{C\equiv N}$); 1604, 1579s($\nu_{C=N}$); 1540, 1504, 1417vs(ν_{CN+CS}), 1247vs(ν_{CN}).

3b. Yield 70%, yellow crystals. Anal. Calcd for $C_{57}H_{62}N_4O_4PdS$: C, 68.1; H, 6.2; N, 5.6; Found: C, 67.7; H, 6.5; N, 5.4.

^{1}H NMR (300 MHz, $CDCl_3$): 8.11 (s, 1H), 7.73 (d br, 2H), 7.64 (m, 4H), 7.53 (AA′BB′ system, $^3J = 8.8$ Hz, 2H), 7.44–7.21 (m, 10H), 6.99 (t, AA′BB′ system, $^3J = 8.5$ Hz, 4H), 6.90 (d br, 1H), 6.60 (dd, $^3J = 8.3$ Hz, $^4J = 2.3$ Hz, 1H), 4.09–4.01 (m, 6H), 2.35 (s, 3H), 1.85 (m, 6H), 1.62–1.28 (m, 18H), 0.89 (m, 3H).

IR (cm^{-1}): 2231w($\nu_{C\equiv N}$); 1604, 1581s($\nu_{C=N}$); 1415vs(ν_{CN+CS}), 1250vs(ν_{CN}).

4a. Yield 70%, yellow crystals. Anal. Calcd for $C_{48}H_{44}N_4O_5PdS$: C, 64.4; H, 5.0; N, 6.3; Found: C, 64.1; H, 5.3; N, 6.0.

^{1}H NMR (300 MHz, $CDCl_3$): 8.11 (s, 1H), 7.75–7.62 (m, 6H), 7.53 (AA′BB′ system, $^3J = 8.8$ Hz, 2H), 7.45–7.33 (m, 7H), 7.25–7.15 (m, 3H), 7.03–6.95 (m, 4H), 6.88 (d br, 1H), 6.60 (dd, $^3J = 8.1$ Hz, $^4J = 2.4$ Hz, 1H), 4.03 (t, $^3J = 6.6$ Hz, 4H), 3.88 (s, 3H), 3.82 (s, 3H), 1.85 (m, 4H), 1.58 (m, 4H).

IR (cm^{-1}): 2224w($\nu_{C\equiv N}$); 1603, 1578s($\nu_{C=N}$); 1506, 1420vs(ν_{CN+CS}), 1247vs(ν_{CN}).

4b. Yield 73%, yellow crystals. Anal. Calcd for $C_{57}H_{62}N_4O_5PdS$: C, 67.0; H, 6.1; N, 5.5; Found: C, 66.8; H, 6.4; N, 5.3.

^{1}H NMR (300 MHz, $CDCl_3$): 8.12 (s, 1H), 7.73 (d br, 2H), 7.64 (m, 4H), 7.53 (AA′BB′ system, $^3J = 8.8$ Hz, 2H), 7.45–7.33 (m, 7H), 7.25–7.15 (m, 3H), 7.03–6.95 (m, 4H), 6.90 (s br, 1H), 6.60 (dd, $^3J = 8.1$ Hz, $^4J = 2.4$ Hz, 1H), 4.09–4.01 (m, 6H), 3.83 (s, 3H), 1.85 (m, 6H), 1.62–1.28 (m, 18H), 0.89 (m, 3H).

IR (cm^{-1}): 2228w($\nu_{C\equiv N}$); 1605, 1579s($\nu_{C=N}$); 1532, 1508, 1374vs(ν_{CN+CS}), 1249vs(ν_{CN}).

5a. Yield 50%, yellow crystals. Anal. Calcd for $C_{47}H_{41}FN_4O_4PdS$: C, 63.9; H, 4.7; N, 6.3; Found: C, 63.7; H, 5.0; N, 6.1.

^{1}H NMR (300 MHz, $CDCl_3$): 8.12 (s, 1H), 7.75–7.62 (m, 6H), 7.55–7.47 (m, 4H), 7.41–7.34 (m, 4H), 7.23 (m, 3H), 7.09–6.97 (m, 6H), 6.60 (dd, $^3J = 8.1$ Hz, $^4J = 2.4$ Hz, 1H), 4.04 (t, $^3J = 6.6$ Hz, 4H), 3.89 (s, 3H), 3.82 (s, 3H), 1.85 (m, 4H), 1.58 (m, 4H).

IR (cm^{-1}): 2234w($\nu_{C\equiv N}$); 1601, 1578s($\nu_{C=N}$); 1538, 1505, 1430vs(ν_{CN+CS}), 1247vs(ν_{CN}).

5b. Yield 55%, yellow crystals. Anal. Calcd for $C_{56}H_{59}FN_4O_4PdS$: C, 66.6; H, 5.9; N, 5.5; Found: C, 66.2; H, 6.3; N, 5.3.

^{1}H NMR (300 MHz, $CDCl_3$): 8.11 (s, 1H), 7.73 (m, 2H), 7.65 (m, 4H), 7.55–7.47 (m, 4H), 7.41–7.34 (m, 4H), 7.23 (m, 3H), 7.09–6.97 (m, 6H), 6.60 (dd, $^3J = 8.4$ Hz, $^4J = 2.2$ Hz, 1H), 4.04 (m, 6H), 1.86 (m, 6H), 1.62–1.28 (m, 18H), 0.89 (m, 3H).

IR (cm^{-1}): 2227w($\nu_{C\equiv N}$); 1604, 1579s($\nu_{C=N}$); 1540, 1506, 1423vs(ν_{CN+CS}), 1250vs(ν_{CN}).

6a. Yield 73%, yellow crystals. Anal. Calcd for $C_{47}H_4ClN_4O_4PdS$: C, 62.7; H, 4.6; N, 6.2; Found: C, 62.6; H, 4.7; N, 6.1.

^{1}H NMR (300 MHz, $CDCl_3$): 8.12 (s, 1H), 7.71–7.60 (m, 6H), 7.51 (t, AA′BB′ system, $^3J = 8.5$ Hz, 4H), 7.43–7.22 (m, 8H), 6.89 (d br, 1H), 6.59 (dd, $^3J = 8.5$ Hz, $^4J = 2.4$ Hz, 1H), 4.05 (m, 4H), 3.89 (s, 3H), 1.86 (m, 4H), 1.58 (m, 4H).

IR (cm^{-1}): 2226w($\nu_{C\equiv N}$); 1602, 1578s($\nu_{C=N}$); 1533, 1505, 1429vs(ν_{CN+CS}), 1246vs(ν_{CN}).

6b. Yield 65%, yellow crystals. Anal. Calcd for $C_{56}H_{59}ClN_4O_4PdS$: C, 65.6; H, 5.8; N, 5.5; Found: C, 65.4; H, 6.4; N, 5.3.

^{1}H NMR (300 MHz, $CDCl_3$): 8.13 (s, 1H), 7.73–7.60 (m, 6H), 7.55–7.47 (m, 4H), 7.42–7.22 (m, 8H), 7.01–6.97 (m, 5H), 6.59 (dd, $^3J = 8.4$ Hz, $^4J = 2.4$ Hz, 1H), 4.05 (m, 6H), 1.86 (m, 6H), 1.62–1.28 (m, 18H), 0.89 (m, 3H).

IR (cm^{-1}): 2223w($\nu_{C\equiv N}$); 1602, 1579s($\nu_{C=N}$); 1537, 1504, 1420vs(ν_{CN+CS}), 1248vs(ν_{CN}).

7a. Yield 53%, yellow crystals. Anal. Calcd for $C_{47}H_4BrN_4O_4PdS$: C, 59.8; H, 4.4; N, 5.9; Found: C, 59.6; H, 4.7; N, 5.7.

^{1}H NMR (300 MHz, $CDCl_3$): 8.11 (s, 1H), 7.73 (d br, 2H), 7.65–7.33 (m, 13H), 7.20 (m, 3H), 6.99 (m, 4H), 6.86 (s br, 1H), 6.59 (dd, $^3J = 8.5$ Hz, $^4J = 2.4$ Hz, 1H), 4.05 (m, 4H), 3.88 (s, 3H), 1.86 (m, 4H), 1.58 (m, 4H).

IR (cm^{-1}): 2225w($\nu_{C\equiv N}$); 1602, 1579s($\nu_{C=N}$); 1538, 1504, 1418vs(ν_{CN+CS}), 1249vs(ν_{CN}).

7b. Yield 55%, yellow crystals. Anal. Calcd for $C_{56}H_{59}BrN_4O_4PdS$: C, 62.8; H, 5.6; N, 5.2; Found: C, 62.4; H, 6.1; N, 5.0.

^{1}H NMR (300 MHz, $CDCl_3$): 8.11 (s, 1H), 7.73–7.60 (m, 6H), 7.55–7.47 (m, 4H), 7.42–7.20 (m, 8H), 7.01–6.97 (m, 5H), 6.61 (dd, $^3J = 8.4$ Hz, $^4J = 2.4$ Hz, 1H), 4.05 (m, 6H), 1.86 (m, 6H), 1.62–1.28 (m, 18H), 0.89 (m, 3H).

IR (cm^{-1}): 2226w($\nu_{C\equiv N}$); 1605, 1578s($\nu_{C=N}$); 1536, 1418vs(ν_{CN+CS}), 1250vs(ν_{CN}).

Acknowledgements The authors acknowledge the financial support from CNCSIS–UEFISCSU, project number PNII–IDEI ID_954/2007 and ID_123/2008.

References

1. Chandrasekar S. Liquid crystals. 2nd ed. Cambridge: University Press; 1992.
2. De Gennes PG, Prost J. The physics of liquid crystals. 2nd ed. Oxford: Clarendon Press; 1993.
3. Donnio B, Guillon D, Deschenaux R, Bruce DW. Metallomesogens, chap 7.9. In: McCleverty JA, Meyer TJ, editors. Comprehensive coordination chemistry II, vol. 7. Oxford: Elsevier; 2003. p. 357–627.
4. Donnio B, Guillon D, Deschenaux R, Bruce DW. Metallomesogens, chap. 12.05. In: Crabtree RH, Mingos DMP, editors. Comprehensive organometallic chemistry III, vol. 12. Oxford: Elsevier; 2006. p. 195–293.
5. Raman R, Jeyamurugan R, Usha Rani R, Baskaran T, Mitu L. Synthesis, characterization, DNA binding, oxidative damage of DNA strand scission, and antimicrobial activities of β-diketone condensed Schiff-base transition metal complexes. J Coord Chem. 2010;63:1629–44.
6. Raman N, Jeyamurugan R, Sakthivel A, Mitu L. Novel metal-based pharmacologically dynamic agents of transition metal(II) complexes: designing, synthesis, structural elucidation, DNA binding and photo-induced DNA cleavage activity. Spectrochim Acta A. 2010;75:88–97.
7. Imran M, Mitu L, Latif S, Mahmood Z, Naimat I, Zaman SS, Fatima S. Antibacterial Co(II), Ni(II), Cu(II) and Zn(II) complexes with biacetyl-derived Schiff bases. J Serb Chem Soc. 2010;75:1075–84.
8. Dogan F, Ulusoy M, Ozturk OF, Kaya I, Salih B. Synthesis, characterization and thermal studies of some tetradentate Schiff base transition metal complexes. J Therm Anal Calorim. 2009;98:785–92.
9. Hogan JL, Imrie CT, Luckhurst GR. Asymmetric dimeric liquid crystals. The preparation and properties of the α-(4-cyanobiphenyl-4′-oxy)-ω-(4-*n*-alkylanilinebenzylidene-4′-oxy)hexanes. Liq Cryst. 1988;3:645–50.
10. Attard GS, Date RW, Imrie CT, Luckhurst GR, Roskilly SJ, Seddon JM, Taylor L. Nonsymmetrical dimeric liquid-crystals—the preparation and properties of the α-(4-cyanobiphenyl-4′-yloxy)-ω-(4-n-alkylanilinebenzylidene-4′-oxy)alkanes. Liq Cryst. 1994;16:529–81.
11. Imrie CT, Henderson PA. Liquid crystal dimers and higher oligomers: between monomers and polymers. Chem Soc Rev. 2007;36:2096–124.
12. Mocanu AS, Ilis M, Dumitrascu F, Ilie M, Cîrcu V. Synthesis, mesomorphism and luminescence properties of palladium(II) and platinum(II) complexes with dimeric Schiff base liquid crystals. Inorg Chim Acta. 2010;363:729–36.
13. Beyer L, Hoyer E, Liebscher J, Hartmann H. Formation of complexes with *N*-acyl-thioureas. Z Chem. 1981;21:81–91.
14. Muhl P, Gloe K, Dietze F, Hoyer E, Beyer L. *N*-acylthioureas—effective extractants for liquid-liquid-extraction of metal-ions. Z Chem. 1986;26:81–94.
15. Koch KR. New chemistry with old ligands: *N*-alkyl- and *N,N*-dialkyl-N′-acyl(aroyl)thioureas in co-ordination, analytical and process chemistry of the platinum group metals. Coord Chem Rev. 2001;216–217:473–88.
16. Seshadri T, Haupt HJ. Thermotropic properties of monosubstituted ferrocene derivatives bearing bidentate *N*-benzoyl-*N*′-arylthiourea ligands—novel building blocks for heterometallic liquid crystal systems. J Mater Chem. 1998;8:1345–50.
17. Deleanu A, Ilis M, Rosu T, Cîrcu V. Complex combinations with *N*-benzoylthiourea derivatives of Pt(II) and Pd(II). Rev Chim (Bucharest). 2006;57:1216–20.
18. Seshadri T, Haupt HJ, Flörke U, Henkel G. Novel cholesteric glassy liquid crystals of monosubstituted ferrocenes: synthesis and selective reflection properties of a dimesogen, and crystal structure of a monomesogen. Liq Cryst. 2007;34:33–47.
19. Tenchiu AC, Ilis M, Dumitrascu F, Whitwood AC, Cîrcu V. Synthesis, characterization and thermal behaviour of ortho-metallated Pd(II) complexes containing *N*-benzoylthiourea derivatives. Polyhedron. 2008;27:3537–44.
20. Cîrcu V, Simonescu CM. Smectic phases of liquid crystals based on dinuclear palladium(II) complexes with carboxylato bridge. Cryst Res Technol. 2010;45:512–6.
21. Cîrcu V, Manaila-Maximean MD, Rosu C, Ilis M, Molard Y, Dumitrascu F. Mesomorphic behaviour and TSDC measurements of ortho-metallated palladium(II) and platinum(II) complexes with S,O-donor co-ligands. Liq Cryst. 2009;36:123–132.
22. Wunderlich B. Thermodynamic description of condensed phases. J Therm Anal Calorim. 2010;102:413–24.
23. van Turnhout J. Thermally stimulated discharge of polymer electrets. Amsterdam: Elsevier; 1975. p. 104–8.
24. Vanderscueren J, Gassiot J. Field-induced thermally stimulated currents. In: Braunlich P, editor. Thermally stimulated relaxation in solids. Berlin: Springer-Verlag; 1979. p. 135–223.
25. Randall JT, Wilkins MHF. Phosphorescence and electron traps.1. The study of trap distributions. Proc R Soc Lond. 1945;A 184:366–89.
26. Costa Ribeiro J. On the thermo-dielectric effect. An Acad Brasil Cienc. 1950;22:325–47.
27. Sharma D, MacDonald JC, Iannacchione GS. Thermodynamics of activated phase transitions of 8CB: DSC and MC calorimetry. J Phys Chem B. 2006;110:16679–84.
28. Sharma D. Calorimetric study of activated kinetics of the nematic and smectic phase transitions in an aligned nano-colloidal liquid crystal+aerosil gel. J Therm Anal Calorim. 2008; 93:899–906.
29. Scaramuzza N, Pagnota MC, Lucchetta DE, Strangi G, Versace C, Ionescu A Th. Thermally induced depolarization currents in a palladium containing metallorganic liquid crystal. Mol Cryst Liq Cryst. 1999;339:83–94.
30. Rosu C, Manaila Maximean D, Bena R, Petrescu E, Klosowicz S, Czuprynski K. Thermally stimulated depolarization currents, optical transmission studies on UV cured polymer dispersed liquid crystal films. Czech J Phys. 2003;53:235–47.
31. Collings PJ, Hird M. Introduction to liquid crystals chemistry and physics. London and New York: Taylor & Francis; 2004.
32. Manaila-Maximean D, Rosu C, Yamamoto T, Yokoyama H. Thermally stimulated depolarization currents on colloidal liquid crystal composite system. Mol Cryst Liq Cryst. 2004;417: 215–26.
33. Rosu C, Manaila-Maximean D, Godinho MH, Almeida PL. Thermally stimulated depolarization currents, optical transmission measurements on liquid crystal/cellulose derivative composite devices. Mol Cryst Liq Cryst. 2003;391:1–11.
34. Dierking I. Textures of liquid crystals. Weinheim: Wiley-VCH Verlag; 2003.
35. Rosu C, Manaila-Maximean D, Paraskos AJ. Thermally stimulated depolarization currents and optical transmission studies on a 3,4 dicyanothiophene based bent-rod liquid crystal. Mod Phys Lett. 2002;B 16:473–83.
36. Douglas IB, Dains FB. Some derivatives of benzoyl and furoyl isothiocyanates and their use in synthesizing heterocyclic compounds. J Am Chem Soc. 1934;56:719–21.